

## Article

# Alkali Recovery of Bauxite Residue by Calcification

Wanzhang Yang <sup>1,2</sup>, Wenhui Ma <sup>1,2</sup>, Pengfei Li <sup>1,2</sup>, Zhanwei Liu <sup>1,2,3,\*</sup> and Hengwei Yan <sup>1,2,3,\*</sup>

<sup>1</sup> State Key Laboratory of Complex Nonferrous Metal Resources Cleaning Utilization, Kunming University of Science and Technology, Kunming 650093, China; yangwz2021@126.com (W.Y.); mwhsilicon@126.com (W.M.); lmn18187512474@126.com (P.L.)

<sup>2</sup> National Engineering Laboratory for Vacuum Metallurgy, Kunming University of Science and Technology, Kunming 650093, China

<sup>3</sup> Aluminum Industry Engineering Research Center of Yunnan Province, Kunming 650093, China

\* Correspondence: zhanwei\_liu@126.com (Z.L.); hengwei\_yan@126.com (H.Y.)

**Abstract:** Bauxite residue (red mud) generated during alumina production is a highly alkaline solid waste. The red mud is mainly stored on land, but it can cause harm to the surrounding environment and human health. The transformation of red mud into soil is a feasible method for the large-scale disposal of red mud, but alkali removal is the key process that controls the transformation of red mud into soil. In this study, the calcification dealkalinization of red mud with a small particle size was carried out below 100 °C. The results show that the sodium in red mud is predominately distributed in small particles, mainly because the lattice alkali and alkali present between the crystals are exposed to the surface of red mud particles by ball milling. The dealkalinization process was controlled by the internal diffusion of the shrinking-core model (SCM), and the apparent activation energy was 23.55 kJ/mol. The dealkalinization rate and the Na<sub>2</sub>O content of dealkalinized red mud reached 92.44% and 0.61%, respectively. The dealkalinization rate increased with increasing reaction time, reactant concentration, and leaching temperature, and this result was consistent with the results of the kinetic study. In addition, calcification enhances the flocculation of particles, so the filtration performance of red mud improved.

**Keywords:** Bayer red mud; dealkalinization; calcification; leaching kinetic



**Citation:** Yang, W.; Ma, W.; Li, P.; Liu, Z.; Yan, H. Alkali Recovery of Bauxite Residue by Calcification. *Minerals* **2022**, *12*, 636. <https://doi.org/10.3390/min12050636>

Academic Editor: Kyoungkeun Yoo

Received: 21 April 2022

Accepted: 12 May 2022

Published: 17 May 2022

**Publisher's Note:** MDPI stays neutral with regard to jurisdictional claims in published maps and institutional affiliations.



**Copyright:** © 2022 by the authors. Licensee MDPI, Basel, Switzerland. This article is an open access article distributed under the terms and conditions of the Creative Commons Attribution (CC BY) license (<https://creativecommons.org/licenses/by/4.0/>).

## 1. Introduction

Bayer red mud is a highly alkaline solid waste generated in the alumina production by the Bayer process; more than 96% of the world's alumina is produced using the Bayer process [1,2]. The red mud output differs with ore grade, technical level, and production method. Approximately between 1 and 1.5 t of Bayer red mud is produced from 1 t of alumina [3–5]. With increasing production of Al<sub>2</sub>O<sub>3</sub> worldwide, the yield of red mud has now exceeded 10 billion tons [6,7]. At present, the comprehensive utilization of red mud is a global problem [8]. In recent years, red mud is mainly disposed by stockpiling [9–11]. However, this method not only leads to occupying land resources but also causes the infiltration of red mud into soil and groundwater. Therefore, this method can lead to security risks and environmental pollution [12–17]. Red mud can be used in adsorbing materials, in building materials, in fillers, and in the recovery of valuable metals [18–30]. However, the high alkalinity of red mud makes it difficult to be used as a raw material for building materials, as the high amounts of alkali can move to the surface of building materials, leading to weak intensity and slag floating. In addition, such high alkalinity results in a high acid consumption and cost during the recovery of precious metals. The high alkalinity of red mud always restricts the development of resource utilization and industrialization. Therefore, the removal of alkali in red mud is necessary.

In recent years, alkali removal from red mud has been studied extensively. Some researchers have summarized the methods for alkali removal from red mud [31]. The

methods for the dealkalinization of red mud mainly include acid leaching [32]; water washing [33,34]; calcification [35,36]; carbon dioxide pressure leaching; and iron hydro-garnet processing, suspension, and carbonation [37–40]. Direct water leaching is a method that mainly studies the effect of multiple factors on the dealkalinization process; these factors include the amount of washing water, the temperature of the washing water, the duration of each washing, and the number of washing cycles. At room temperature, when red mud's liquid/solid ratio is 5:1, and after it has been soaked 1 d and washed five times, 75% of the free alkali in red mud can be removed. However, the chemically bonded alkali of red mud cannot be removed. Acid leaching could remove more than 95% of alkali under the following conditions: a reaction temperature of 80 °C, an oxalic-acid content of 15%, a liquid/solid ratio of 4 mL/g, and a reaction time of 40 min. Oxalic acid significantly damages the structure of cancrinite in the red mud, and it can selectively remove sodium in red mud. The content of sodium oxide in the alkali residue is less than 0.5%, but it may also dissolve magnesium and aluminum. Experiments were carried out for the dealkalinization of alkaline red mud with hot water and the CaO water-bath method. The results show that the dealkalinization rate was less than 75% under the following conditions: a CaO quantity of 10%, a leaching temperature of 95 °C, and three leaching stages. Some researchers used CO<sub>2</sub> gas to react with red-mud slurry in order to remove alkali from alkaline red mud. The dealkalinization rate was about 50% under the following conditions: CO<sub>2</sub> airflow of 0.3 L/min, a liquid/solid ratio of 7 mL/g, a reaction temperature of 50 °C, a reaction pressure 4 MPa, and a reaction time of 2 h. However, the process was difficult to operate due to a high pressure. These methods have their own advantages and disadvantages, and they have not been widely applied in the industry.

In this study, the calcification dealkalinization of red mud with a small particle size was carried out below 100 °C. Compared with the traditional calcification method, the calcification dealkalinization of red mud with a small particle size can provide a higher alkali removal rate at a lower temperature and shorter time, and the dealkalinized red mud has better filtration properties. The sodium content in red mud of different particle sizes and the alkali-removal kinetics induced by adding CaO were studied. In addition, the effects of different factors, such as leaching temperature, calcium-oxide content, leaching reaction time, and liquid/solid ratio on the dealkalinization of red mud, were studied. This study provides technical support for the alkali removal of Bayer red mud and a scientific reference for the sustainable and healthy development of the alumina industry.

## 2. Materials and Methods

### 2.1. Materials

The raw material of red mud was collected from an aluminum company in Henan Province, China. The sample was analyzed by X-ray fluorescence (XRF) spectroscopy (Rigaku ZSX Priums, JEOL, Akishima-shi, Japan), and the results are shown in Table 1.

**Table 1.** The main chemical composition of red mud.

Element	Al <sub>2</sub> O <sub>3</sub>	SiO <sub>2</sub>	CaO	Fe <sub>2</sub> O <sub>3</sub>	Na <sub>2</sub> O	TiO <sub>2</sub>	Others
Content (%)	27.36	23.21	14.90	11.08	8.63	6.25	8.57

Table 1 shows the chemical composition of the sample. It is apparent that the main alkaline composition is sodium, not potassium. Therefore, in this study, the strength of alkali was measured by determining the content of Na<sub>2</sub>O in red mud. The content of Na<sub>2</sub>O in red mud is 8.63%. The Na<sub>2</sub>O content is an important index to measure the alkalinity of red mud, and its content is generally between 2% and 10%. Therefore, the Na<sub>2</sub>O content of red mud is higher. Furthermore, it also contains many other useful metals such as iron, aluminum, titanium, calcium, etc.

The X-ray diffraction (XRD) (X'Pert Pro MPD, PANalytical B.V., Heracles Almelo, The Netherlands) pattern of a red-mud sample is shown in Figure 1.

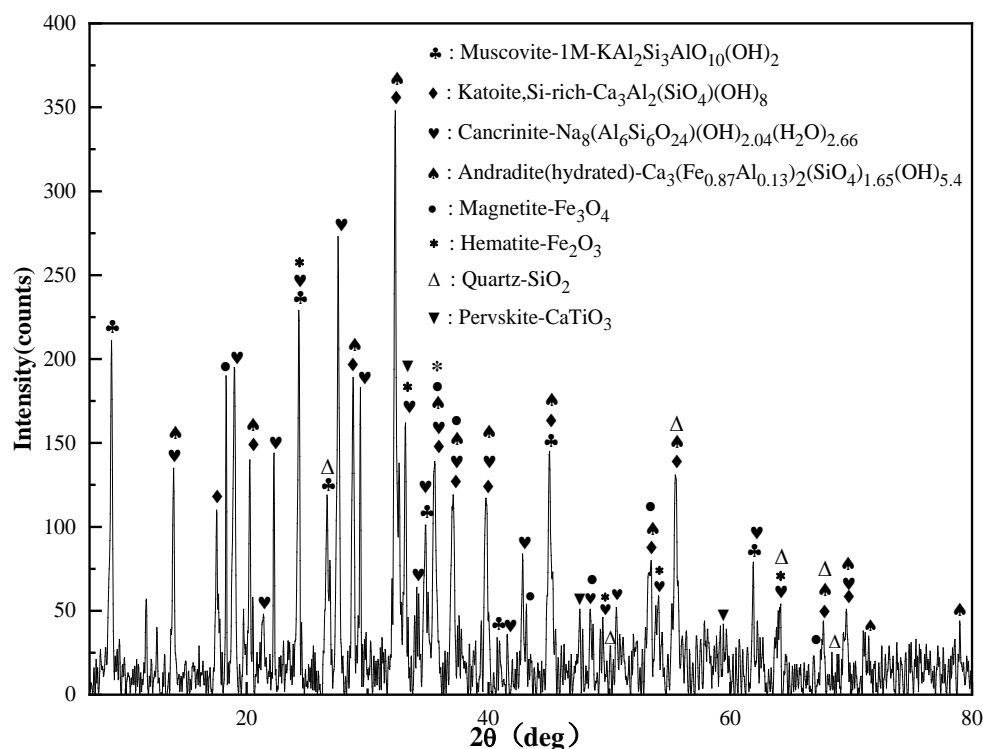


**Figure 1.** XRD pattern of the red-mud sample.

It can be seen from Figure 1 that the main minerals in the red-mud sample are muscovite, katoite, cancrinite, andradite, magnetite, hematite, and quartz. Above all, it is found that alkali mainly exists in cancrinite. If we rely only on water leaching, it is difficult to remove the alkali.

The surface morphology of samples was detected by scanning electron microscopy (SEM) (JSM-IT800, JEOL, Akishima-shi, Japan) equipped with energy-dispersive X-ray spectroscopy (EDS). The results are shown in Figure 2; it was found that the sample of red mud contains irregular needle, columnar, and granule particles. In addition, some of the red-mud particles are aggregated. The results of the SEM-EDS analysis show that the red mud is mainly composed of aluminum, calcium, iron, sodium, silicon, and titanium. The distribution of these elements is not uniform. This is also consistent with the chemical composition shown in Table 1.

## 2.2. Methods

The experimental procedure is shown in Figure 3. The red-mud sample was first treated by ball milling, and it was dried with a loft drier at a temperature of 120 °C for no less than 1 h. Second, red mud and a blend with a specific molar ratio of calcium oxide were added to a Teflon beaker. Third, an alkali-recovery experiment was carried out in a HH-S1s constant-temperature water bath. The temperature of the water bath was controlled within  $\pm 0.5$  °C. Finally, a solid cake and filtrate were obtained by filtration using a SHB-III A vacuum filter. The obtained solids were washed with deionized water and dried in a laboratory oven at 105 °C for subsequent analysis. The content of alkali in the solids was determined by atomic adsorption spectrometry (AAS) (AA-3600, Shanghai Metash Instruments Co., Ltd., Shanghai, China).

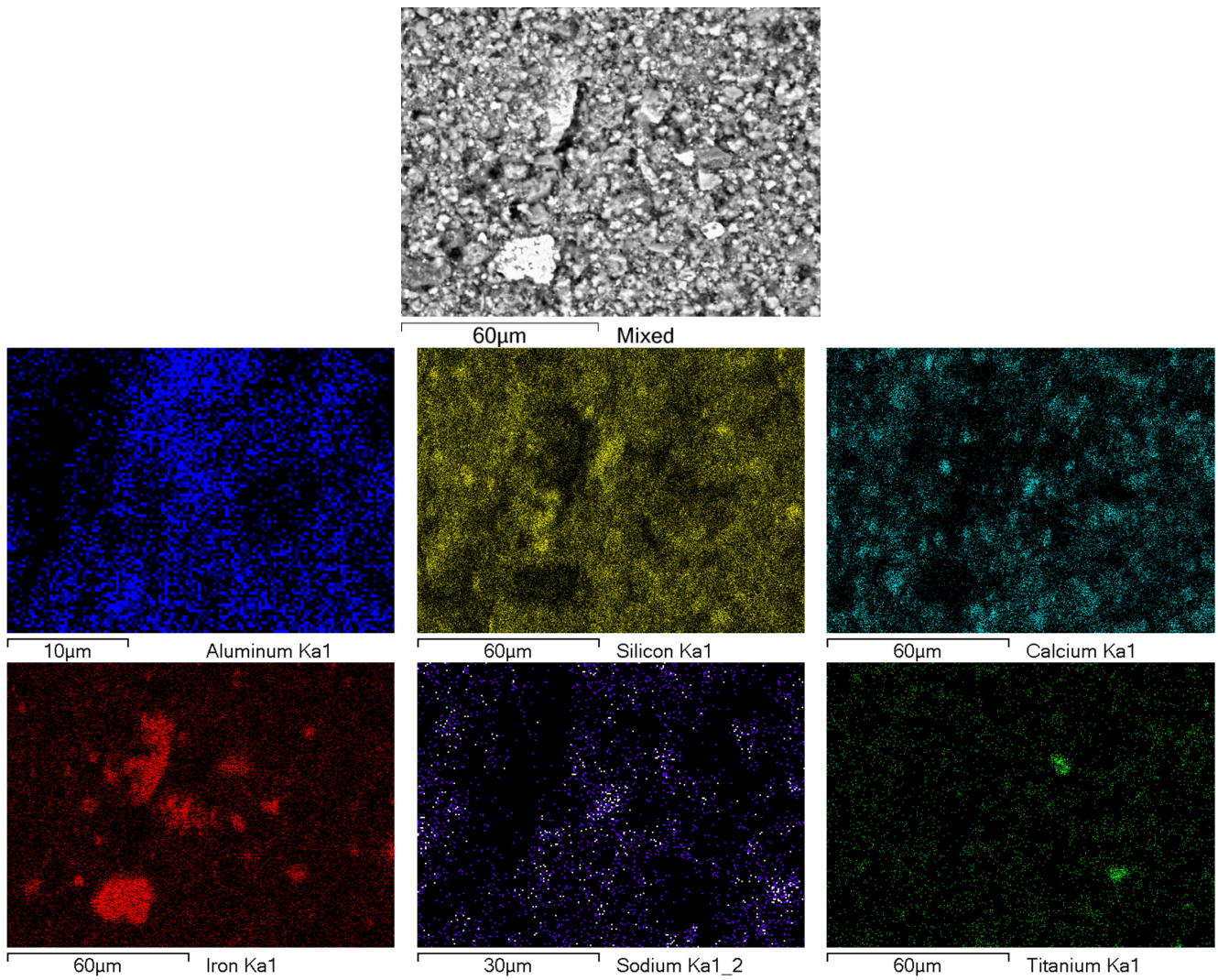


Figure 2. SEM-EDS analysis of the red-mud sample.

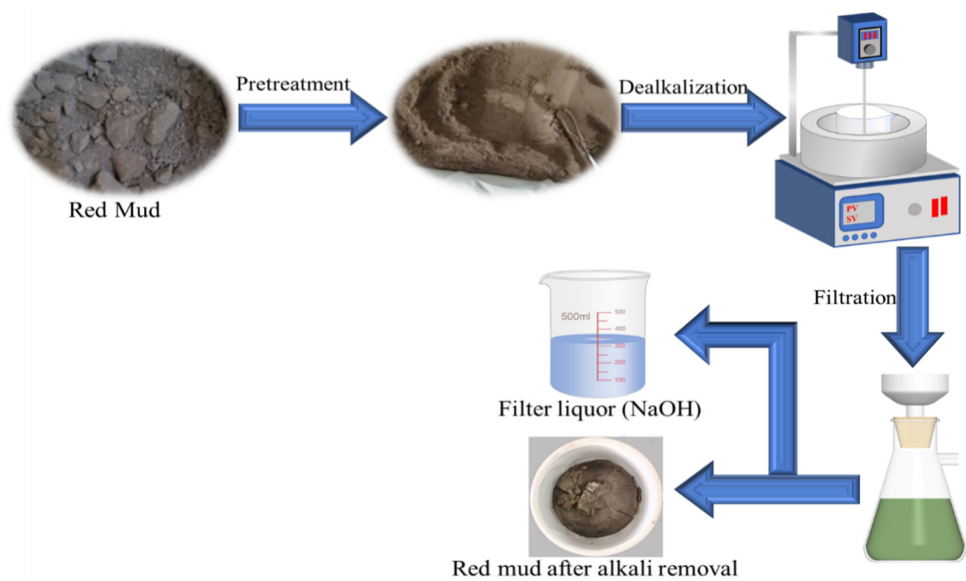


Figure 3. Experimental procedure.

### 3. Results and Discussion

#### 3.1. Analysis of Red Mud with Different Particle Sizes

To further study how to improve the dealcalization rate of red mud, red mud with different granularities was studied in detail. The agglomeration of red mud is obvious during direct screening. Therefore, the raw material was divided into different particle sizes by wet screening. The content of Na<sub>2</sub>O in red mud with different particle sizes was analyzed by AAS, and the results are shown in Table 2. The sodium is more distributed in particles whose size is less than 48 microns. The lattice alkali and the alkali between the crystals are exposed to the surface of the red-mud particles by grinding, so the sodium in red mud is more distributed in smaller particles.

**Table 2.** The content of Na<sub>2</sub>O in red mud with different particle sizes.

Particle Size	>106 μm	75–106 μm	48–75 μm	<48 μm
Content (%)	3.90	3.50	3.28	8.07

The XRD pattern of the red mud sample with different particle sizes is shown in Figure 4; it was found that the phase composition of red mud with different granularities is very complex. The main minerals that contain sodium are cancrinite and muscovite. Although the diffraction peak intensities of Na<sub>6</sub>Ca<sub>2</sub>Al<sub>6</sub>Si<sub>6</sub>O<sub>24</sub>(CO<sub>3</sub>)<sub>2</sub>·2H<sub>2</sub>O and (K,Na)(Al,Mg,Fe)<sub>2</sub>(Si<sub>3.1</sub>Al<sub>0.9</sub>)O<sub>10</sub>(OH)<sub>2</sub> were different in the red-mud sample with different particle sizes, the phase containing sodium is not obviously different in red mud with different particle sizes. In addition, the iron phase is mainly distributed in red mud with particles sizes smaller than 75 microns.

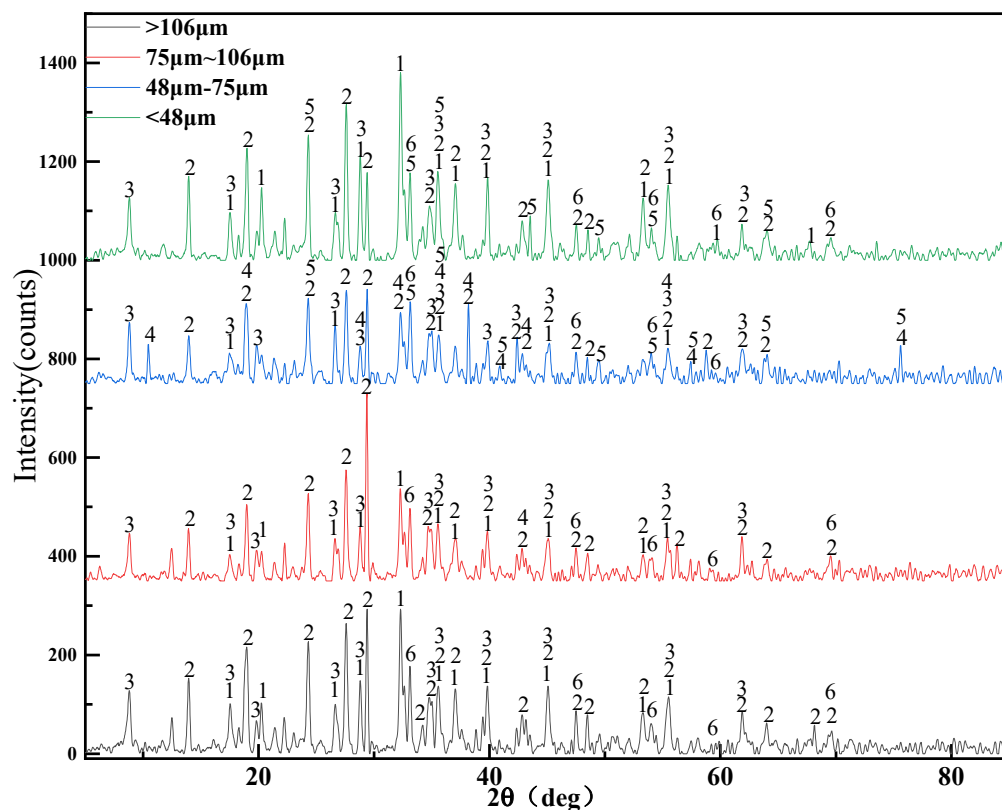


**Figure 4.** XRD pattern of the red-mud sample with different particle sizes (1—Ca<sub>3</sub>Al<sub>2</sub>(SiO<sub>4</sub>)(OH)<sub>8</sub>; 2—Na<sub>6</sub>Ca<sub>2</sub>Al<sub>6</sub>Si<sub>6</sub>O<sub>24</sub>(CO<sub>3</sub>)<sub>2</sub>·2H<sub>2</sub>O; 3—(K,Na)(Al,Mg,Fe)<sub>2</sub>(Si<sub>3.1</sub>Al<sub>0.9</sub>)O<sub>10</sub>(OH)<sub>2</sub>; 4—Fe<sub>7</sub>Si<sub>8</sub>O<sub>22</sub>(OH)<sub>2</sub>; 5—Fe<sub>2</sub>O<sub>3</sub>; 6—CaTiO<sub>3</sub>).

The SEM-EDS analysis of red mud with different particle sizes is shown in Figure 5. The morphology of red mud with different particle sizes is different. The sample of red mud with particle sizes greater than 75 microns contains mainly irregular particles. However, the sample of red mud with particle sizes less than 75 microns contains distinctly irregular cylinders and spicules. The results of elemental distribution show that the sodium exists with silicon, calcium, and aluminum at different positions in red mud.

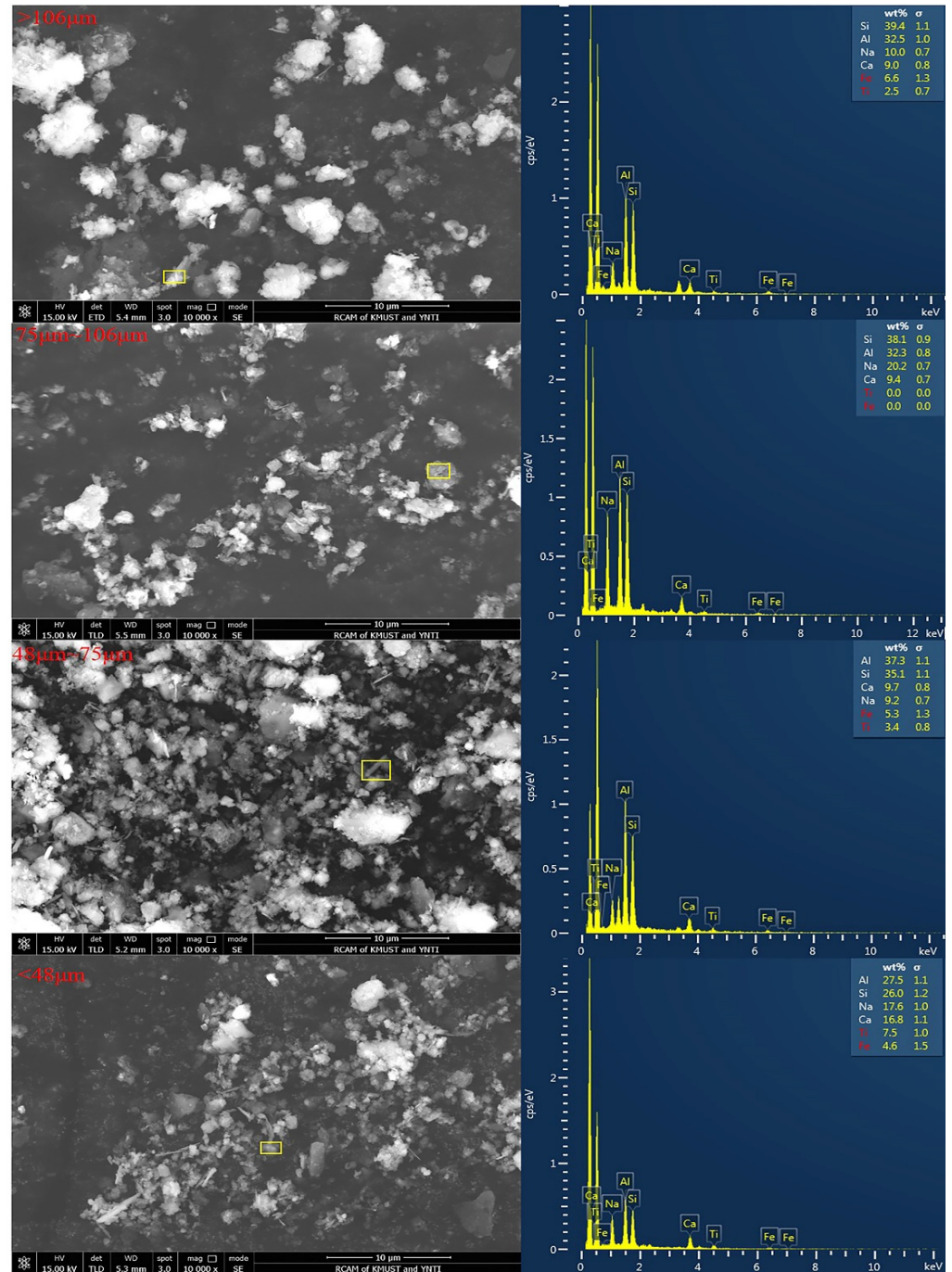


Figure 5. SEM-EDS analysis of red mud with different particle size.

### 3.2. Kinetic Analysis of Dealkalization Reaction

It is important to build a quantitative measurement of the leaching kinetics to verify the dealkalization process. The experimental data of the leaching process can be described with a shrinking-core model (SCM) [41]. Under different control conditions, the kinetics equations can be simplified as follows:

Liquid boundary layer diffusion control:

$$k_a t = \alpha \tag{1}$$

Chemical reaction control:

$$k_b t = \left[ 1 - (1 - \alpha)^{\frac{1}{3}} \right] \tag{2}$$

Internal diffusion control:

$$k_c t = \left[ 1 - 2\frac{\alpha}{3} - (1 - \alpha)^{\frac{2}{3}} \right] \tag{3}$$

where  $k_a$  is the rate constant of liquid boundary layer diffusion control,  $k_b$  is the rate constant of chemical reaction,  $k_c$  is the rate constant of internal diffusion,  $t$  is the reaction time (h), and  $\alpha$  is the dealkalization rate (%).

Three controlling steps of the SCM were studied at different dealkalization temperatures (60 °C, 70 °C, 80 °C, 90 °C, and 95 °C). The results are shown in Figures 6–8.

According to Figures 6–8, it was found that the control of internal diffusion fit the dealkalization data well at different temperatures. The dealkalization process was controlled by internal diffusion, so the major factor was the internal diffusion rate of the calcium hydroxide solution as it moved into the interior of red-mud particles. The internal diffusion rate increased with increasing reactant concentration, leaching time, and leaching temperature. The plots of  $\ln(K_a)$  with temperature are shown in Figure 9.

The correlation coefficient ( $R^2$ ) was over 0.94 at different leaching temperatures. The apparent activation energy ( $E_a$ ) of the leaching process was calculated as 23.55 kJ/mol.

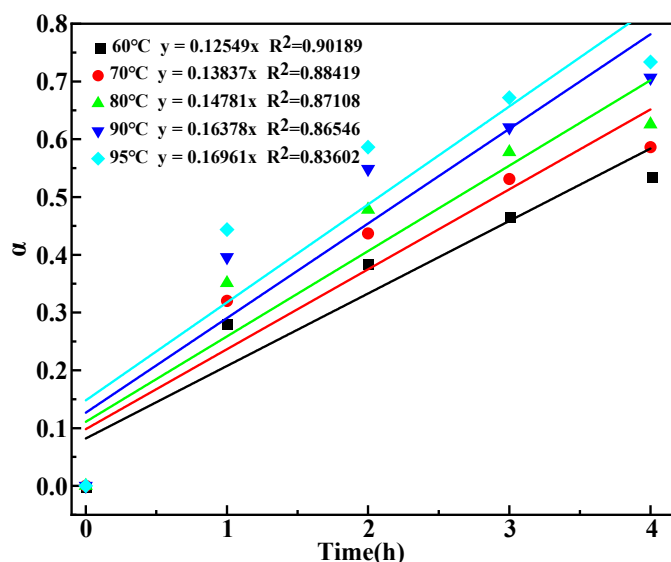


Figure 6. Plots of  $\alpha$  versus time at different temperatures.

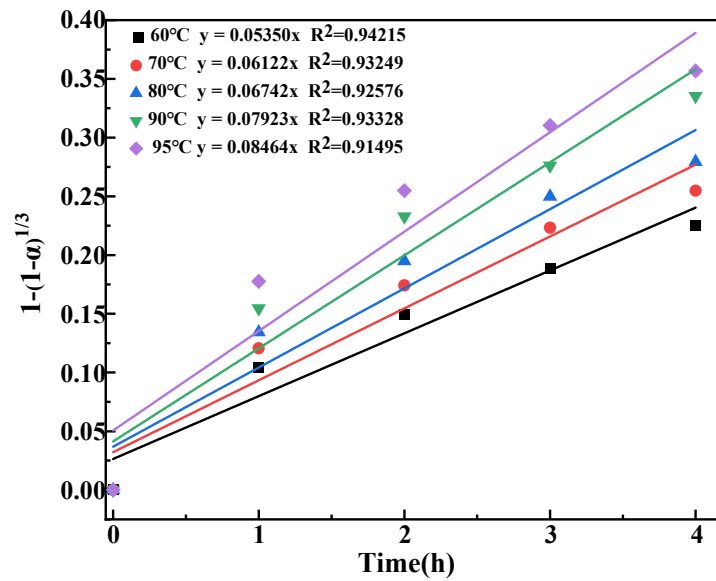


Figure 7. Plots of  $1 - (1 - \alpha)^{1/3}$  versus time at different temperatures.

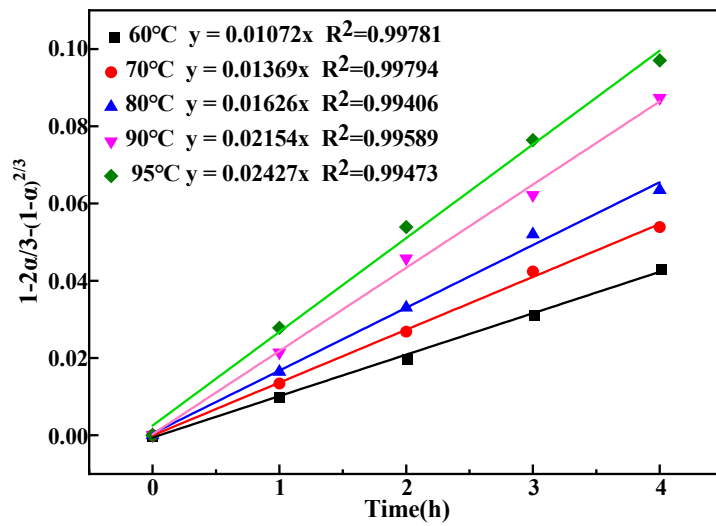


Figure 8. Plots of  $1 - 2\alpha/3 - (1 - \alpha)^{2/3}$  versus time at different temperatures.

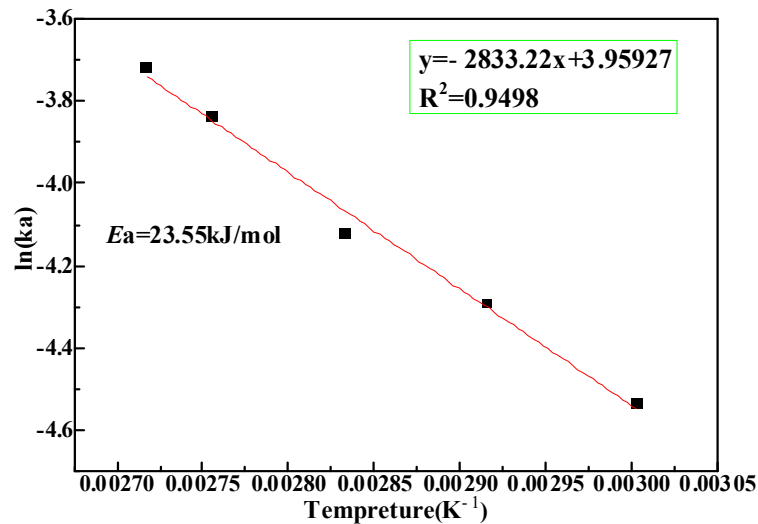


Figure 9. Plots of  $\ln(Ka)$  versus temperature of leaching process.

### 3.3. Effect of Reaction Temperature

The effect of reaction temperature on the dealcalization rate is shown in Figure 10 under the following conditions: CaO/Na<sub>2</sub>O = 4.5 (quality ratio), a reaction time of 2 h, and a liquid/solid ratio of 4 mL/g.

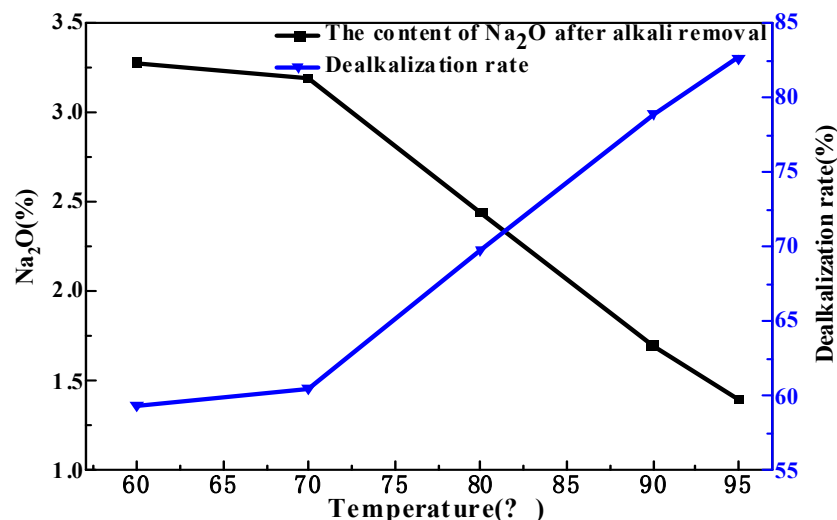


Figure 10. Effect of reaction temperature on dealcalization rate.

Figure 10 shows that the effect of reaction temperature on the dealcalization rate was apparent. The dealcalization rate increased with the increase in reaction temperature. With the increase in reaction temperature, the dealcalization reaction proceeded more thoroughly. When the reaction temperature increased from 60 °C to 95 °C at a reaction time of 2 h, the dealcalization rate increased from 59.35% to 83.65%. Therefore, the optimum reaction temperature is 95 °C.

### 3.4. Effect of Reaction Time

The effect of reaction time on the dealcalization rate is shown in Figure 11 under the following conditions: a reaction temperature of 95 °C and a liquid/solid ratio of 4 mL/g.

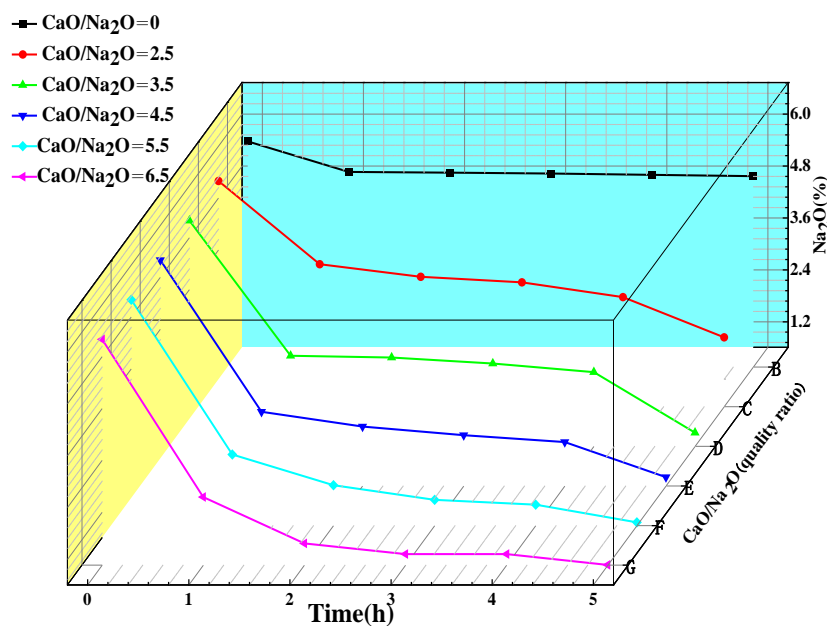


Figure 11. Effect of reaction time on dealcalization rate.

As shown in Figure 11, the dealkalinization rate of red mud increased with time when the quality ratios of CaO/Na<sub>2</sub>O were 0, 2.5, 3.5, 4.5, 5.5, and 6.5. The larger the ratio of CaO/Na<sub>2</sub>O, the greater the effect of reaction time on the dealkalinization rate. The increase in the dealkalinization rate was unremarkable when CaO/Na<sub>2</sub>O = 0. The increase in the dealkalinization rate was obvious at a low reaction time, and it became mild at a high reaction time when CaO/Na<sub>2</sub>O = 2.5, 3.5, 4.5, 5.5, and 6.5. After reaction for 1 h, the dealkalinization rate of red mud could reach 33.05%, 56.74%, 60.17%, 61.37%, and 62.58%, respectively. Then, when the reaction time was increased from 2 h to 5 h, the dealkalinization rate increased from 38.03%, 54.33%, 69.44%, 73.56%, and 80.94% to 72.61%, 88.60%, 89.96%, 91.57%, and 92.44%, respectively. The dealkalinization rate of red mud could reach 92.44% and the content of Na<sub>2</sub>O could reach 0.61% under the following conditions: a reaction time of 5 h and CaO/Na<sub>2</sub>O = 6.5. However, given the costs of long experiments and other factors to consider, we could only choose 2 h as the reaction time. In addition, it was found that the amount of CaO would influence the dealkalinization rate. Therefore, it is necessary to further study how the addition of calcium oxide impacts alkali removal.

### 3.5. Effect of Calcium Oxide

The effect of CaO on the dealkalinization rate of red mud is shown in Figure 12 under the following conditions: a reaction temperature of 95 °C; reaction times of 1, 2, 3, and 4 h; and a liquid/solid ratio of 4 mL/g.

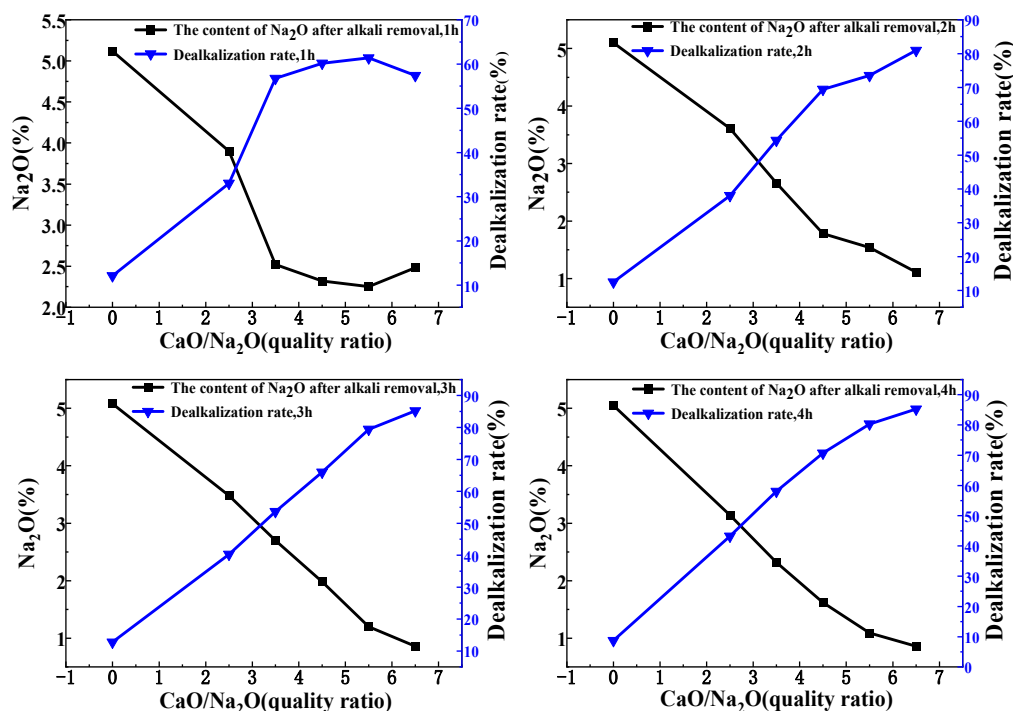


Figure 12. Effect of CaO on dealkalinization rate.

Figure 12 shows that the effect of CaO on the dealkalinization rate was apparent. The dealkalinization rate of red mud increased with the increase in calcium oxide dosage. The dealkalinization rate reached 33.05% when the reaction time was 1 h and CaO /Na<sub>2</sub>O = 3.5. Then, the tendency of the dealkalinization rate to change became mild with an increase in the calcium-oxide dosage. The dealkalinization rate reached 69.44% when the reaction time was 2 h and CaO/Na<sub>2</sub>O = 4.5. Then, the tendency of the dealkalinization rate to change became mild with the increase in calciumoxide dosage. The dealkalinization rate reached 79.40% when the reaction time was 3 h and CaO/Na<sub>2</sub>O = 5.5. Then, the tendency of the dealkalinization rate to change became mild with the increase in calcium-oxide dosage. The dealkalinization rate reached 80.31% when the reaction time was 4 h and CaO /Na<sub>2</sub>O = 5.5.

Then, the dealkalization rate reached 85.24% when  $\text{CaO}/\text{Na}_2\text{O} = 6.5$ . These results show that the dealkalization rate of red mud changed as calcium-oxide dosages were increased for different lengths of time; accordingly, larger calcium-oxide dosages require longer reaction times. There must be sufficient reaction time to ensure the red mud's complete reaction, but in light of economic considerations, a very high calcium-oxide dosage is unsustainable. Therefore, the amount of  $\text{CaO}$  is more appropriate when the  $\text{CaO}/\text{Na}_2\text{O} = 4.5$ .

### 3.6. Effect of Liquid/Solid Ratio

The liquid/solid ratio is an important factor. The effect of the liquid/solid ratio on the dealkalization rate is shown in Figure 13 under the following conditions: a reaction time of 2 h, a leaching temperature of  $95\text{ }^\circ\text{C}$ , and  $\text{CaO}/\text{Na}_2\text{O} = 4.5$ .

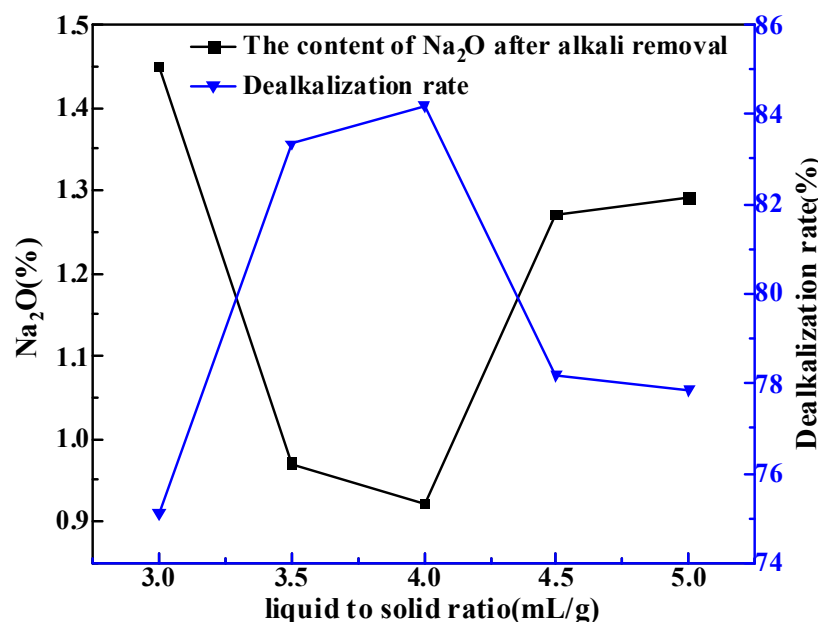
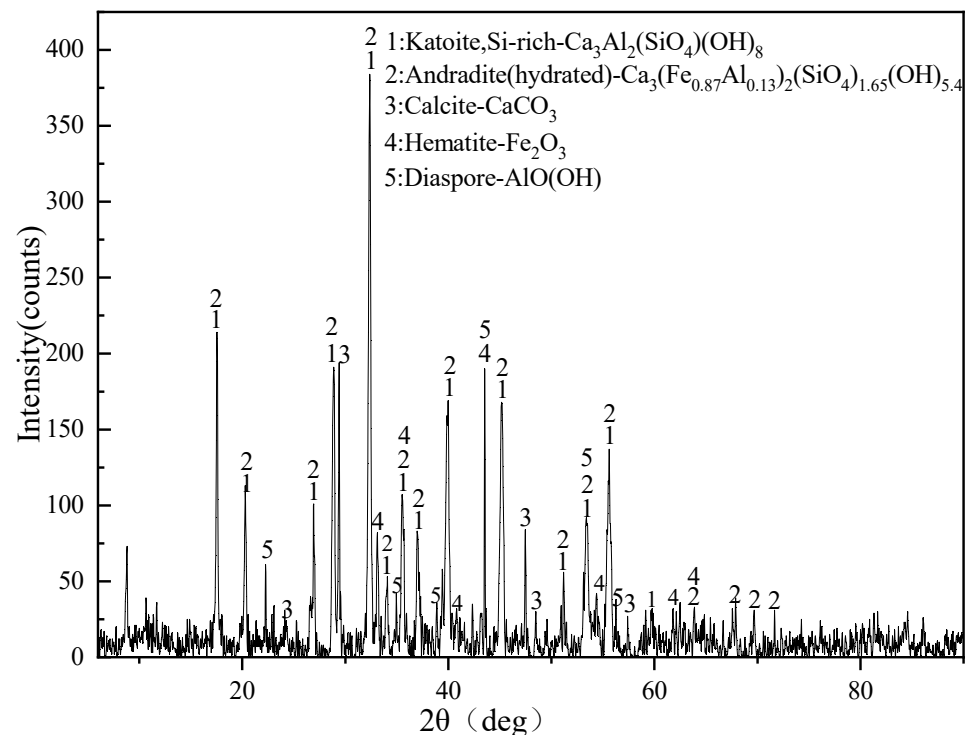


Figure 13. Effect of liquid to solid ratio on dealkalization rate.

Figure 13 shows that the effect of the liquid/solid ratio on the dealkalization rate was apparent. The dealkalization rate of red mud increased to the maximum value and then decreased as the liquid/solid ratio increased. The highest rate of dealkalization reached 84.20% when the liquid/solid ratio = 4.0 mL/g. According to the kinetic analysis described above, the concentration of the reactant is proportional to the rate of alkali removal. When the liquid/solid ratio is low, the amount of liquid is insufficient to dissolve the reactant and the viscosity is too large, which is not conducive to the reaction. The reactant concentration is too small in a high liquid/solid ratio, which is obviously not conducive to the reaction; this point is consistent with the results of the kinetic study.

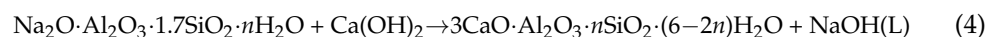
### 3.7. XRD Analysis of Red Mud after Dealkalization

XRD analysis of red mud after dealkalization is shown in Figure 14 under the following conditions: a reaction temperature of  $95\text{ }^\circ\text{C}$ , a reaction time of 2 h,  $\text{CaO}/\text{Na}_2\text{O} = 4.5$ , and a liquid/solid ratio of 4 mL/g.



**Figure 14.** The XRD pattern of the slag after dealcalization.

It is shown that the main minerals in the slag after dealcalization are katoite, andradite, calcite, hematite, and diaspore. Above all, the alkali in red mud is mainly a chemically bonded alkali in the form of sodium silicate slag ( $\text{Na}_2\text{O} \cdot \text{Al}_2\text{O}_3 \cdot n\text{SiO}_2 \cdot m\text{H}_2\text{O}$ ), except for some attached alkali. The dealcalization process of adding CaO to red mud is expected to change the sodium silicon slag in red mud into calcium silicon slag ( $3\text{CaO} \cdot \text{Al}_2\text{O}_3 \cdot n\text{SiO}_2 \cdot (6-2n)\text{H}_2\text{O}$ ) under hydrothermal condition. The  $\text{Na}_2\text{O}$  in sodium silicon slag entered the solution to achieve the goal of dealcalization. Except for the main reaction, the other alkali components in red mud, such as  $\text{Na}_2\text{CO}_3$  and  $\text{Na}_2\text{SiO}_3$ , can also react with  $\text{Ca}(\text{OH})_2$  to form insoluble substances and enter red mud. The above reaction process is verified by the results shown in Figure 14.



### 3.8. Filtration Performance of Dealcalized Red Mud

It was found that the addition of CaO significantly affected the filtration process. The higher the calcium-oxide dosage, the higher the dealcalization rate. The filtration process takes less time and is better. Figure 15 shows the difference in different calcium oxide dosages after air pump filtration. Figure 15A shows the results obtained without adding calcium oxide. Figure 15B shows the experimental results obtained with the increase in calcium-oxide dosage. Obviously, the samples without calcium oxide after filtration have a high moisture content and are very sticky.

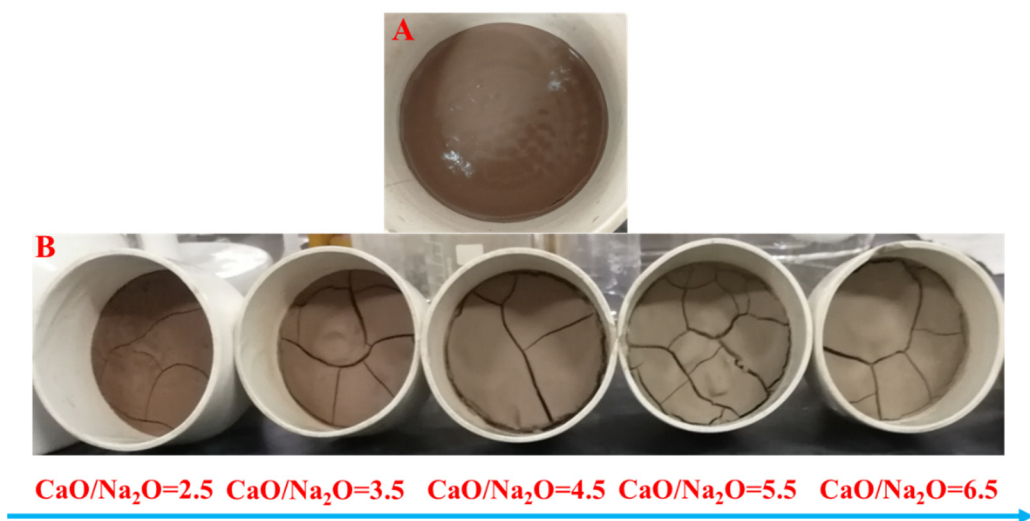


**Figure 15.** Effect of CaO addition on the filtration performance of red mud. (A) without adding calcium oxide, (B) with adding calcium oxide.

The effect of CaO addition on the sedimentation rate of red mud is shown in Figure 16.

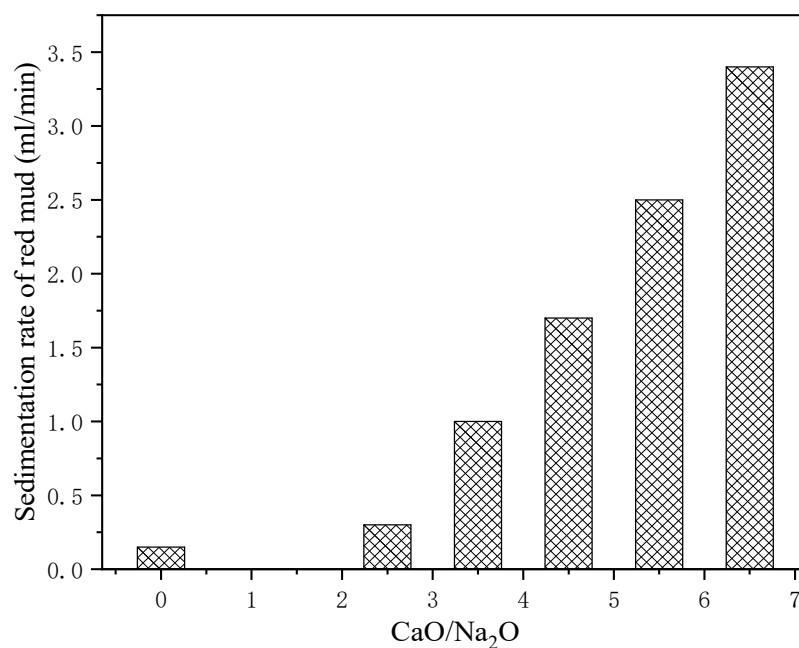


**Figure 16.** Effect of CaO addition on the sedimentation rate of red mud.

Figure 16 shows that as the calcium-oxide dosage increases, the sedimentation rate of red mud increases.

The effect of CaO addition on the moisture content of red-mud filter cake is shown in Figure 17.

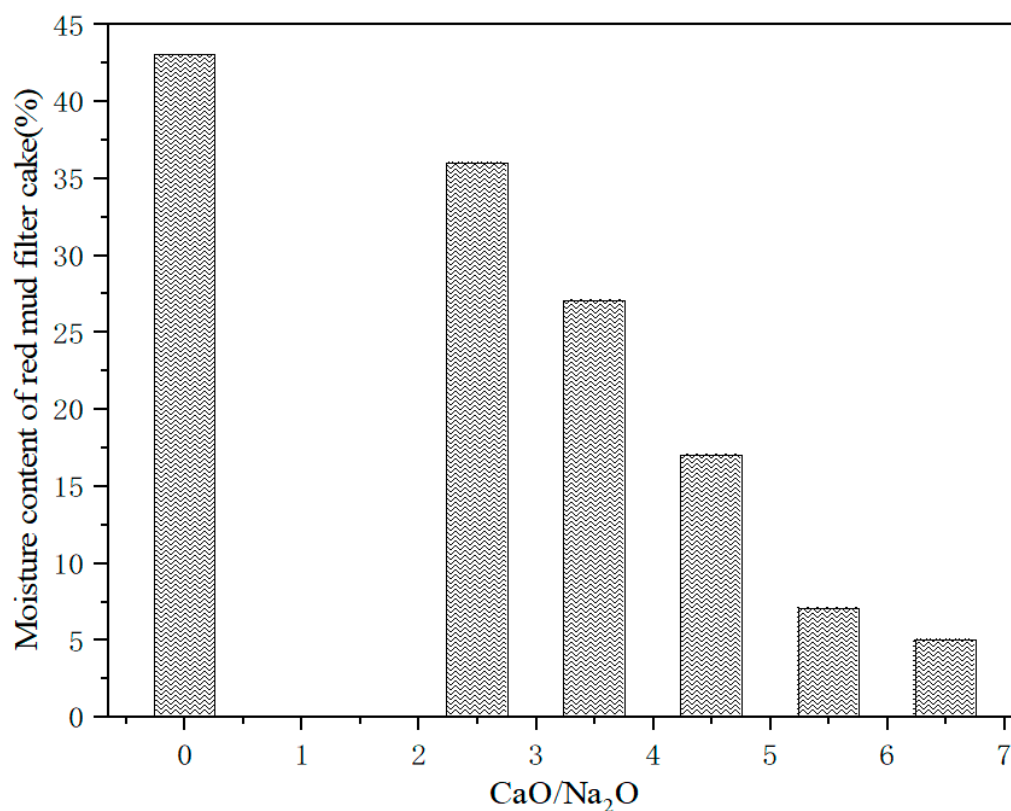


**Figure 17.** Effect of CaO addition on the moisture content of red-mud filter cake.

Figure 17 shows that as the calcium-oxide dosage increases, the moisture content of red mud-filter cake decreases.

To further analyze the reasons, we analyzed the red mud before and after dealkalization by SEM, and the results are shown in Figure 18.

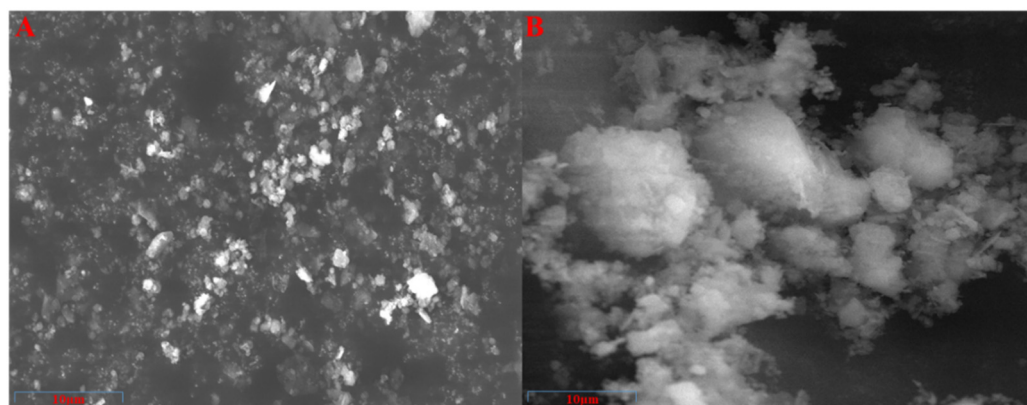


**Figure 18.** SEM analysis of red mud. (A) red mud before dealkalization, (B) red mud after dealkalization.

Compared with the red mud before alkali removal, the red-mud particles formed a cluster after alkali removal—i.e., the red mud flocculated after the removal of alkali. This formation occurred mainly because the calcium ions acted as a bridge between the different particles. This also explains why adding calcium oxide to remove alkali is more effective in filtration. Therefore, adding lime to dealkalize enhances the flocculation of red mud and improves the filtration performance of red mud.

#### 4. Conclusions

The results obtained in this study indicate that the lattice alkali and alkali present between the crystals are exposed to the surface of the red-mud particles by ball milling, and the sodium water leaching solution in red mud is predominately distributed in small particles. The dealkalization process was controlled by the internal diffusion of SCM, and the apparent activation energy was 23.55 kJ/mol. The sodium silicon slag can react with calcium oxide to produce calcium silicon slag ( $3\text{CaO}\cdot\text{Al}_2\text{O}_3\cdot n\text{SiO}_2\cdot(6-2n)\text{H}_2\text{O}$ ). It was found that the dealkalization rate of red mud increased as reaction time, reactant concentration, and leaching temperature increased; this observation is consistent with the kinetics results. Under the condition of a reaction time of 5 h,  $\text{CaO}/\text{Na}_2\text{O} = 6.5$ , liquid/solid ratio of 4 mL/g, a leaching temperature of 95 °C, the dealkalization rate and the content of  $\text{Na}_2\text{O}$  could reach 92.44% and 0.61%, respectively. In addition, adding CaO to remove alkali enhanced the flocculation of red-mud particles and improved the filtration performance of red mud.

**Author Contributions:** Conceptualization, Z.L. and W.M.; methodology, Z.L.; validation, Z.L., P.L. and W.M.; formal analysis, W.Y.; investigation, W.Y.; resources, H.Y.; data curation, P.L.; writing—original draft preparation, W.Y. and P.L.; writing—review and editing, W.Y. and P.L.; visualization, Z.L.; supervision, H.Y.; project administration, W.M.; funding acquisition, Z.L. All authors have read and agreed to the published version of the manuscript.

**Funding:** This work was supported financially by the National Natural Science Foundation of China (No. 22068021 and No. 52064030), Yunnan industrial talent project (YNQR-CYRC-2018-003) and the Project of State Key Research and Development Plan (2019YFC1904205).

**Conflicts of Interest:** The authors declare no conflict of interest.

#### References

1. Klauber, C.; Gräfe, M.; Power, G. Bauxite residue issues: II. options for residue utilization. *Hydrometallurgy* **2011**, *108*, 11–32. [[CrossRef](#)]
2. Liu, Z.; Zong, Y.; Li, H.; Jia, D.; Zhao, Z. Selectively recovering scandium from high alkali Bayer red mud without impurities of iron, titanium and gallium. *J. Rare Earths* **2017**, *35*, 896–905. [[CrossRef](#)]
3. Zhu, S.; Zhu, D.; Wang, X. Removal of fluorine from red mud (bauxite residue) by electrokinetics. *Electrochim. Acta* **2017**, *242*, 300–306. [[CrossRef](#)]
4. Sahu, M.K.; Patel, R.K. Removal of safranin-O dye from aqueous solution using modified red mud: Kinetics and equilibrium studies. *RSC Adv.* **2015**, *5*, 78491–78501. [[CrossRef](#)]
5. Hua, Y.; Heal, K.V.; Friesl-Hanl, W. The use of red mud as an immobiliser for metal/metalloid-contaminated soil: A review. *J. Hazard. Mater.* **2017**, *325*, 17–30. [[CrossRef](#)]
6. Evans, K. The History, Challenges, and New Developments in the Management and Use of Bauxite Residue. *J. Sustain. Met.* **2016**, *2*, 316–331. [[CrossRef](#)]
7. Liu, Y.; Naidu, R.; Ming, H. Red mud as an amendment for pollutants in solid and liquid phases. *Geoderma* **2011**, *163*, 1–12. [[CrossRef](#)]
8. Power, G.; Gräfe, M.; Klauber, C. Bauxite residue issues: I. Current management, disposal and storage practices. *Hydrometallurgy* **2011**, *108*, 33–45. [[CrossRef](#)]
9. Liu, Z.; Li, H.; Huang, M.; Jia, D.; Zhang, N. Effects of cooling method on removal of sodium from active roasting red mud based on water leaching. *Hydrometallurgy* **2017**, *167*, 92–100. [[CrossRef](#)]
10. Ye, N.; Yang, J.; Liang, S.; Hu, Y.; Hu, J.; Xiao, B.; Huang, Q. Synthesis and strength optimization of one-part geopolymer based on red mud. *Constr. Build. Mater.* **2016**, *111*, 317–325. [[CrossRef](#)]
11. Man, K.; Zhu, Q.; Li, L.; Liu, C.; Xing, Z. Preparation and performance of ceramic filter material by recovered silicon dioxide as major leached component from red mud. *Ceram. Int.* **2017**, *43*, 7565–7572. [[CrossRef](#)]
12. Li, Y.; Li, W.; Xiao, Q.; Song, S.; Naidu, R. Acid mine drainage remediation strategies: A review on migration and source controls. *Miner. Met. Process.* **2018**, *35*, 148–158. [[CrossRef](#)]
13. Jones, B.; Haynes, R.; Phillips, I. Addition of an organic amendment and/or residue mud to bauxite residue sand in order to improve its properties as a growth medium. *J. Environ. Manag.* **2012**, *95*, 29–38. [[CrossRef](#)] [[PubMed](#)]
14. Mayes, W.; Burke, I.; Gomes, H.; Anton, Á.; Molnár, M.; Feigl, V.; Ujaczki, É. Advances in understanding environmental risks of red mud after the ajka spill, hungary. *J. Sustain. Metall.* **2016**, *2*, 332–343. [[CrossRef](#)]
15. Luo, M.; Qi, X.; Zhang, Y.; Ren, Y.; Tong, J.; Chen, Z.; Hou, Y.; Yeerkebai, N.; Wang, H.; Feng, S.; et al. Study on dealkalization and settling performance of red mud. *Environ. Sci. Pollut. Res.* **2016**, *24*, 1794–1802. [[CrossRef](#)]

16. Akinci, A.; Artir, R. Characterization of trace elements and radionuclides and their risk assessment in red mud. *Mater. Charact.* **2008**, *59*, 417–421. [[CrossRef](#)]
17. Gu, H.; Wang, N.; Liu, S. Characterization of Bayer red mud from Guizhou, China. *Min. Met. Explor.* **2012**, *29*, 169–171. [[CrossRef](#)]
18. Liu, R.-X.; Poon, C.S. Utilization of red mud derived from bauxite in self-compacting concrete. *J. Clean. Prod.* **2016**, *112*, 384–391. [[CrossRef](#)]
19. Ujaczki, É.; Zimmermann, Y.; Gasser, C.; Molnár, M.; Feigl, V.; Lenz, M.; Zimmermann, Y.; Gasser, C. Red mud as secondary source for critical raw materials—purification of rare earth elements by liquid/liquid extraction. *J. Chem. Technol. Biotechnol.* **2017**, *92*, 2683–2690. [[CrossRef](#)]
20. Nan, X.L.; Zhang, T.A.; Wu, Y.Q.; Dou, Z.H. A study on absorption of low-concentration SO<sub>2</sub> by Bayer red mud. *J. Northeast. Univ.* **2010**, *31*, 986–989.
21. Ghosh, I.; Guha, S.; Balasubramaniam, R.; Kumar, A.R. Leaching of metals from fresh and sintered red mud. *J. Hazard. Mater.* **2011**, *185*, 662–668. [[CrossRef](#)] [[PubMed](#)]
22. De Michelis, I.; Ferella, F.; Varelli, E.F.; Vegliò, F. Treatment of exhaust fluorescent lamps to recover yttrium: Experimental and process analyses. *Waste Manag.* **2011**, *31*, 2559–2568. [[CrossRef](#)] [[PubMed](#)]
23. Liang, G.; Chen, W.; Nguyen, A.V.; Nguyen, T.A.H. Red mud carbonation using carbon dioxide: Effects of carbonate and calcium ions on goethite surface properties and settling. *J. Colloid Interface Sci.* **2018**, *517*, 230–238. [[CrossRef](#)] [[PubMed](#)]
24. Tsakiridis, P.; Oustadakis, P.; Katsiapi, A.; Perraki, M.; Agatzini, L.S. Synthesis of TiO<sub>2</sub> nano-powders prepared from purified sulphate leach liquor of red mud. *J. Hazard. Mater.* **2011**, *194*, 42–47. [[CrossRef](#)] [[PubMed](#)]
25. Li, X.; Xiao, W.; Liu, W.; Liu, G.-H.; Peng, Z.-H.; Zhou, Q.; Qi, T.-G. Recovery of alumina and ferric oxide from Bayer red mud rich in iron by reduction sintering. *Trans. Nonferrous Met. Soc. China* **2009**, *19*, 1342–1347. [[CrossRef](#)]
26. Tam, P.W.Y.; Panias, D.; Vassiliadou, V. Sintering Optimisation and Recovery of Aluminum and Sodium from Greek Bauxite Residue. *Minerals* **2019**, *9*, 571. [[CrossRef](#)]
27. Li, X.-B.; Wang, Y.-L.; Zhou, Q.-S.; Qi, T.-G.; Liu, G.-H.; Peng, Z.-H.; Wang, H.-Y. Transformation of hematite in diasporic bauxite during reductive Bayer digestion and recovery of iron. *Trans. Nonferrous Met. Soc. China* **2017**, *27*, 2715–2726. [[CrossRef](#)]
28. Chaikin, L.; Shoppert, A.; Valeev, D.; Loginova, I.; Napol'Skikh, J. Concentration of Rare Earth Elements (Sc, Y, La, Ce, Nd, Sm) in Bauxite Residue (Red Mud) Obtained by Water and Alkali Leaching of Bauxite Sintering Dust. *Minerals* **2020**, *10*, 500. [[CrossRef](#)]
29. Zhou, R.; Liu, X.; Luo, L.; Zhou, Y.; Wei, J.; Chen, A.; Tang, L.; Wu, H.; Deng, Y.; Zhang, F.; et al. Remediation of Cu, Pb, Zn and Cd-contaminated agricultural soil using a combined red mud and compost amendment. *Int. Biodeterior. Biodegrad.* **2017**, *118*, 73–81. [[CrossRef](#)]
30. Vafeias, M.; Bempelou, A.; Georgala, E.; Davris, P.; Balomenos, E.; Panias, D. Leaching of Ca-Rich Slags Produced from Reductive Smelting of Bauxite Residue with Na<sub>2</sub>CO<sub>3</sub> Solutions for Alumina Extraction: Lab and Pilot Scale Experiments. *Minerals* **2021**, *11*, 896. [[CrossRef](#)]
31. Xue, S.; Kong, X.; Zhu, F.; Hartley, W.; Li, X.; Li, Y. Proposal for management and alkalinity transformation of bauxite residue in China. *Environ. Sci. Pollut. Res.* **2016**, *23*, 12822–12834. [[CrossRef](#)] [[PubMed](#)]
32. Li, W.; Zhu, X.B. Dealkalization of red mud with oxalic acid. *Bull. Ceram. Soc.* **2016**, *35*, 1283–1286.
33. Zhang, L.G.; Wang, G.Z.; Duan, L.C. Preliminary dealkalization of red mud by washing process. *Inorg. Chem.* **2011**, *43*, 57–58.
34. Zhu, X.; Li, W.; Guan, X. An active dealkalization of red mud with roasting and water leaching. *J. Hazard. Mater.* **2015**, *286*, 85–91. [[CrossRef](#)]
35. Zhang, G.L.; Li, S.C.; Zhang, X.Y.; Wang, Z.K. Comparison study on different de-alkalization process of red mud by bayer process. *Inorg. Chem. Ind.* **2012**, *44*, 40–42.
36. Zhu, X.F.; Zhang, T.A.; Wang, Y.X.; Lv, G.Z.; Zhang, W.G. Recovery of alkali and alumina from Bayer red mud by the calcification-carbonation method. *Int. J. Min. Met. Mater.* **2016**, *23*, 257–268. [[CrossRef](#)]
37. Zhang, R.; Zheng, S.L.; Ma, S.H.; Zhang, Y. Recovery of alumina and alkali in Bayer red mud by the formation of andradite-grossular hydrogarnet in hydrothermal process. *J. Hazard. Mater.* **2011**, *189*, 827–835. [[CrossRef](#)]
38. Yu, Z.L.; Shi, Z.X.; Chen, Y.M.; Niu, Y.J.; Wang, Y.X.; Wan, P.Y. Red-mud treatment using oxalic acid by UV irradiation assistance. *Trans. Nonferr. Met. Soc.* **2012**, *22*, 456–460. [[CrossRef](#)]
39. Wang, X.; Zhang, Y.; Liu, J.; Hu, P.; Meng, K.; Lv, F.; Tong, W.; Chu, P.K. Dealkalization of Red Mud by Carbide Slag and Flue Gas. *CLEAN—Soil Air Water* **2017**, *46*, 1700634. [[CrossRef](#)]
40. Wang, X.; Zhang, Y.; Lv, F.; An, Q.; Lu, R.; Hu, P.; Jiang, S. Removal of alkali in the red mud by SO<sub>2</sub> and simulated flue gas under mild conditions. *Environ. Prog. Sustain. Energy* **2014**, *34*, 81–87. [[CrossRef](#)]
41. Zhou, B.; Cao, S.; Chen, F.; Zhang, F.; Zhang, Y. Recovery of Alkali from Bayer Red Mud Using CaO and/or MgO. *Minerals* **2019**, *9*, 269. [[CrossRef](#)]